JOURNAL OF AIRCRAFT
Vol. 41, No. 6, November–December 2004

Analysis of the Flight Attempt by Samuel Langley's "Great Aerodrome"

Lorenzo Auriti*
National Research Council Canada, Ottawa, Ontario K1A 0R6, Canada
and
James DeLaurier†
University of Toronto, Toronto, Ontario M3H 5T6, Canada

Aerodynamic and structural analyses of Samuel Langley's Great Aerodrome were completed to determine the cause of its failure on launch. Launches of the Aerodrome were attempted in 1903 from a houseboat, resulting in immediate failures and plunges into the Potomac River. Before these launch attempts, Langley had become established as a distinguished scientist with an excellent reputation. He conducted pioneering work in aircraft research by designing flying scale models and creating the first successful engine-powered unmanned airplane. The success of the models added to the mystery of the Great Aerodrome's failure. Speculation throughout aviation history produced many hypotheses about its failure and also provided the motivation for this study. The wing's aerodynamic properties were required for the analysis, and so a scale model was constructed for wind-tunnel testing. The aerodynamic loads found were applied to an ANSYS finite element model of the front-starboard wing to analyse the wing structurally. The results showed that the Aerodrome was not capable of flight as launched off of the houseboat. The wing loads found were higher than the structure could support. The analysis also showed that the wing deformed substantially, resulting in a twist with the trailing edge turned up.

Nomenclature

A	=	area of beam cross section
AR	=	aspect ratio
$(AR)_i$	=	effective aspect ratio
$(AR)_o$	=	aspect ratio of the Aerodrome wing with no gap
b	=	wing span
$C_{L\alpha}$	=	slope of wing lift curve
C_{L_0}	=	lift coefficient at $\alpha = 0$
$(C_{L\alpha})_\infty$	=	slope of infinite aspect ratio lift curve
$C_{M_{ac}}$	=	pitching moment coefficient about aerodynamic center
c	=	mean aerodynamic chord
$c(y)$	=	chord distribution along the span
E	=	elastic modulus
I	=	moment of inertia of a beam cross section
L	=	length of a beam in buckling analysis
P_{cr}	=	critical buckling force
q	=	dynamic pressure
r	=	radius of gyration $(I/A)^{0.5}$
V	=	aircraft airspeed
y	=	y position along a semispan or wing gap width
$\delta(y)$	=	wing twist distribution along the span
ρ	=	air density, 1.2 kg/m^3, assumed
σ_{cr}	=	critical buckling stress
σ_y	=	yield stress

Introduction

THE purpose of this paper is to assess whether the piloted pioneer airplane designed by Samuel Langley was capable of sustained flight, provided its launch had been perfect. The airplane in question, shown in Fig. 1, was an evolution from successful unpiloted scale models, one of which is shown in Fig. 2. Figure 2 also shows the means for launching, which was a catapult mounted on the top of a houseboat moored in the Potomac River. Furthermore, note that the wings are significantly distorted, which illustrates the aeroelastic compliance typical of Langley's designs.

At the time of these tests (1894–1903), Samuel Langley was the Secretary for the Smithsonian Institution in Washington, D.C. His career as a scientist had been distinguished by fundamental studies of atmospheric and solar physics. To this day, a unit for solar flux is measured in langleys. However, he also had a long-term interest in aerodynamics and aeronautics, and had performed force measurements on plates moving through air, as well as flight experiments with rubber-band powered models. A summary and critique of this work may be found in Ref. 1. When he assumed his appointment at the Smithsonian, he then had the resources to pursue his aeronautical interests at a higher level. The aircraft configuration he settled on was a tandem-wing design with an aft-mounted tail unit for stability and control. (These airplanes were called Aerodromes by Langley.) Also, as Figs. 2 and 3 show, the wings had a significant dihedral angle to provide lateral stability. In fact, Langley's design philosophy was to provide the airframe with inherent stability, independent of pilot input. This was illustrated by the stable free-flight performance of Aerodrome 5, which flew successfully in 1896. This was a large model (wingspan of 4 m) powered by a compact steam engine. After launching, it executed large spiral climbing turns for more than 1 min until the fuel was expended. Note that this was the first successful flight of an engine-powered airplane. Because of the solid reputation of Langley in the scientific community, and the reporting of this by Alexander Graham Bell, Langley's accomplishment clearly elucidated the viability of heavier-than-air flight.

From this success, it is easy to understand that Langley felt he had the technological key for achieving humanity's age-old dream of heavier-than-air piloted flight, and the motivation for pursuing this was provided by the Spanish–American War in 1898. It was proposed that an airplane could provide a mobile elevated platform for observation, and funding was issued by the U.S. Government for building a prototype. As it turned out, the war was over before the airplane was completed, but the project was continued. The airplane, called the Great Aerodrome, was completed in 1903 and readied for

Received 10 September 2003; revision received 6 November 2003; accepted for publication 11 November 2003.

*Research Associate, Flight Research Laboratory, Building U-61, 1200 Montreal Road.

†Professor, Institute for Aerospace Studies, 4925 Dufferin Street. Associate Fellow AIAA.

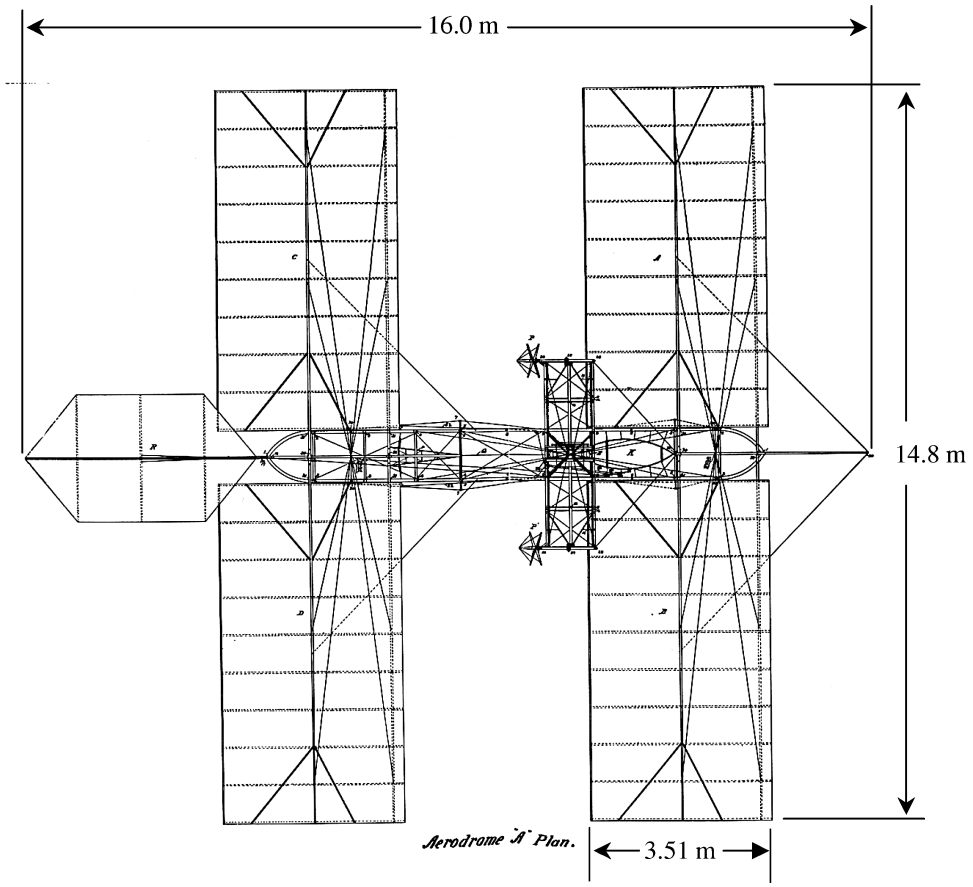

Fig. 1 Great aerodrome plan view.

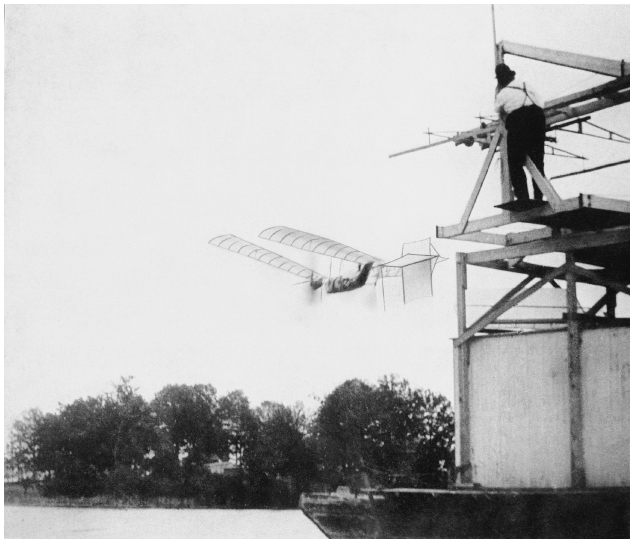

Fig. 2 Launch of a successful unpiloted scale model.

testing. As was done with the scale models, it was launched from a houseboat-mounted catapult. However, the Aerodrome quickly dove into the river, with no flight being achieved (Fig. 3). It was concluded that the crash was due to a faulty launch, and the airplane was repaired for another attempt on 8 December 1903. In this case, the Aerodrome rose nose up and again crashed into the Potomac River. Nine days later the Wright brothers flew, and Langley's quest for flight was over.

Only still photos of the tests exist. There was no motion-picture footage, although the technology was available at that time. Such footage might have greatly helped to explain the reasons for the failures. As it is, the root causes for the crashes have remained in

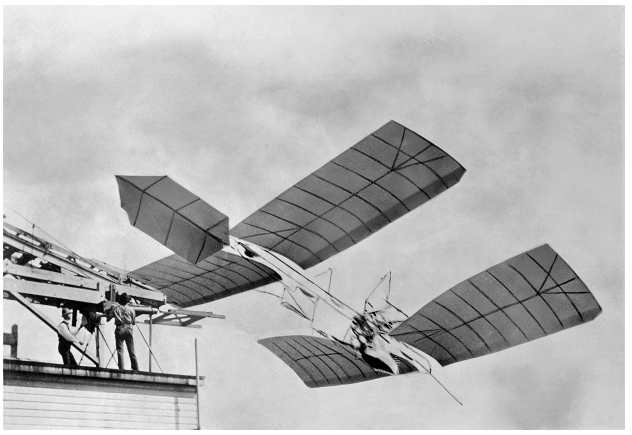

Fig. 3 First attempt to launch the Aerodrome.

question. Based on the success of the models, the Smithsonian Institution took the stance that the aircraft was, in fact, capable of sustained flight and that the failure was due to shortcomings in the launching mechanism. This notion was reinforced when the aircraft was rebuilt by Glenn Curtiss in 1914 and successfully flown in 1914 and 1915. In this instance, the aircraft was mounted on floats and took off from Lake Keuka. However, as noted by the Wright brothers,[2] who were in an intense patent litigation with Curtiss regarding the invention of lateral control, many modifications were made to the rebuilt Great Aerodrome. In particular, the wing structure was considerably strengthened. Therefore, the question remains as to whether or not the original aircraft could have sustained flight, given a perfect launch.

As aeronautical technology progressed, including an understanding of aeroelastic effects, the notion grew that the Great Aerodrome's failure was due to wing divergence.[3] By 1942, in fact, the

Smithsonian Institution concluded that the Great Aerodrome was a fundamentally flawed design, and the Wright Flyer took its rightful place as the first successful human-carrying airplane. Still, no proper aeroelastic analysis was ever performed on the Great Aerodrome, and it was felt by the authors that such an exercise would provide a service to aviation history by finally settling the issue of the aircraft's flight capability.

Specifications of the Langley Aerodrome

Samuel Langley and his assistant, Charles M. Manly, carefully documented their work.[4] Most of the following specifications for the Langley Aerodrome are found in Ref. 4. The fuselage of the Aerodrome (or main frame) was made mostly out of steel tubing. It was not covered like today's aircraft, but was left as an open structure. The power source for the aircraft was a 52-hp internal-combustion radial engine driving two propellers, one on each side of the main frame. The propellers were mounted to another component called the transverse frame. It was attached perpendicular to the mainframe and housed the drive shafts from the centrally mounted engine. The mass of the entire aerodrome, including Langley's assistant Charles M. Manly as the pilot, was 386 kg.

The aerodynamic surfaces of the aircraft consisted of the two identical wings as well as vertical and horizontal tails. These surfaces were covered with a cloth called percaline, and they were the only aerodynamic surfaces that could be controlled by the pilot. The wings were placed in a tandem monoplane configuration, and each of these wings had its two halves separated by an uncovered gap where the open structure of the fuselage was located. The wings were made as light as possible because Langley and Manly calculated that each wing-half should have a mass of 13.6 kg (the mass of the front and rear wings would then total 54.4 kg). Amazingly, they achieved their goal and each half was approximately 13.2 kg for a rectangular planform of 6.87 by 3.51 m and a wing area of 24.1 m.^{2} (Ref. 4).

Figure 1 shows that the wings had a main spar, a front spar, and a trailing-edge spar. Each of these spars was made of hollow spruce. The main and front spars had circular cross sections, and the trailing-edge spar had a D-shaped section. Figure 4, from the Ref. 4, shows the spars and their cross sections. The main and front spars' cross sections were tapered along their lengths. At the point where they met the fuselage, their cross section was similar to the large end of the main spar in Fig. 4. They began to taper at the midpoint of their lengths down to the small end shown in Fig. 4. The trailing edge was 21 mm wide and 13 mm high, with a D-shaped cross section that remained constant along the wing. Diagonal cross braces ran from the point where the main spar met the third rib, to the tip rib, to help support the cloth covering. The diagonal cross braces were the same dimensions and cross section as the main spar at the large end.

Each wing half had 10 ribs, also made from spruce. Figure 5 shows a side view of a rib and cross sections at various points. The ribs had six-sided hollow cross sections at the points where they met the main and front spars. They also had four-sided hollow box-shaped cross sections at the trailing edge. The two end ribs (the one closest to the fuselage and the one at the tip) had slightly larger cross sections than the other eight ribs. Small partitions, approximately

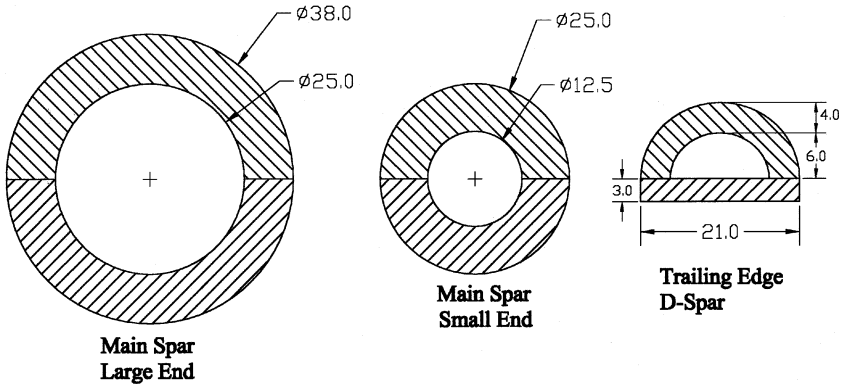

Fig. 4 Spars and their cross sections, dimensions in millimeters.

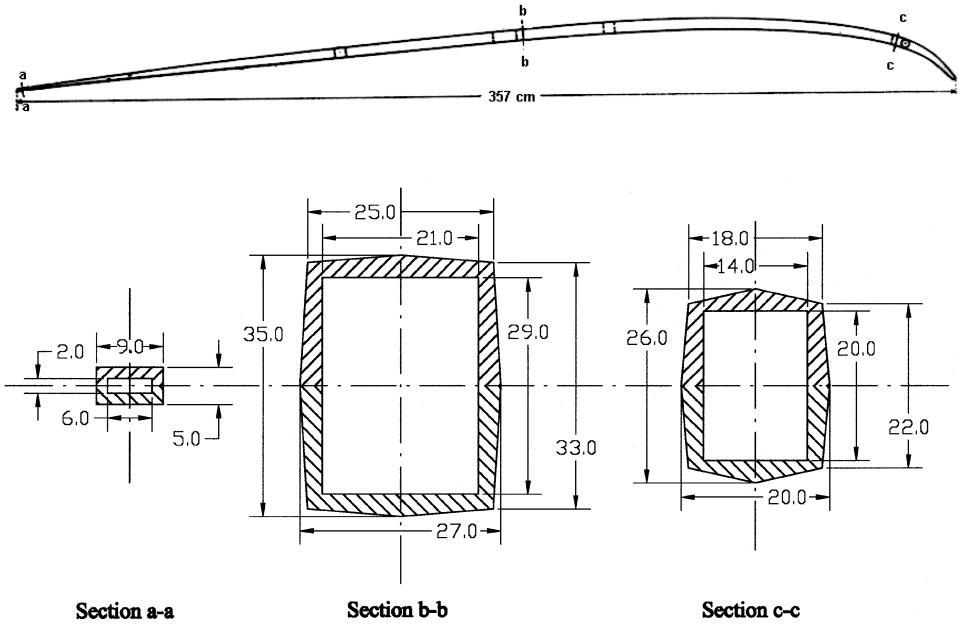

Fig. 5 Rib and cross sections, dimensions in millimeters.

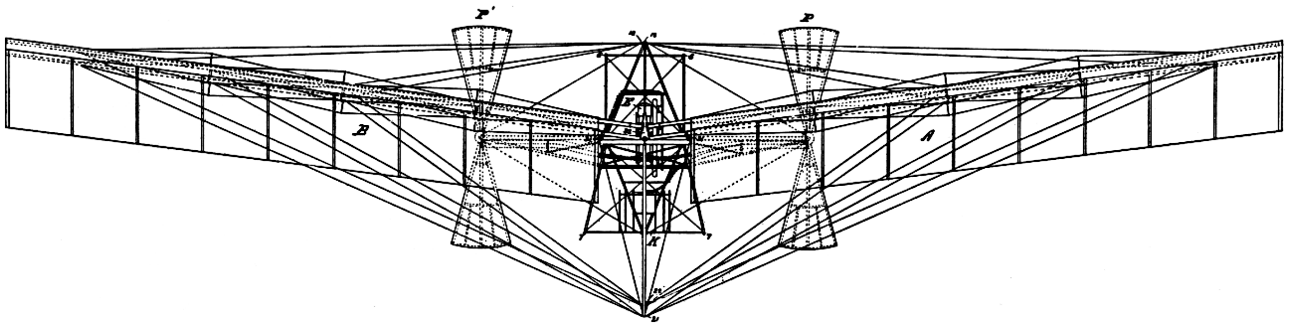

Fig. 6 Front view of the Langley aerodrome.

1 mm thick, were inserted and glued every 76 mm inside the ribs. They were installed to prevent the ribs from crushing. This was an idea that Langley and Manly got from "analyzing the structure of bamboo poles.[4]" Longer blocks of wood were also glued inside the ribs at the points where they attached to the main spar, as well as at the front end where they met with the front spar. Likewise, blocks were glued inside at the points where the diagonal cross braces were attached.

Langley and Manly relied heavily on a system of guy wires to provide strength and stiffness in the wings of the Aerodrome. They felt that this was the lightest possible way to stiffen the wing. Figure 6 is a front view of the Langley Aerodrome, which shows the guy-wire system. The main guy wires extended from posts on the frame of the fuselage to various points on the wing. Six wires extended from the lower guy post to the bottom of the wing, and four extended from the upper guy post to the top of the wing. Another wire, called the drift wire, or drag wire, extended from a post at the center of the fuselage to support the drag force on the wing. This is seen in the plan view of the aircraft in Fig. 1. The front view in Fig. 6 also shows the trusslike system of wires that reinforced the front and main spars. Three upper and three lower guy posts were connected to the spars for these wires to pass over. Each of the 10 ribs was likewise individually guyed. A wire ran from the leading edge, over a 305-mm (12-in.) post that extended from the rib at the point where it met the main spar, to the trailing edge. A wire was also used to create the leading edge. It ran along the tips of each rib. Its main purpose was to support the cloth covering in between the ribs.

Aerodynamic Studies

Initially it was thought that thin-airfoil theory[5] could be used to determine the aerodynamic characteristics of the Langley Aerodrome airfoil, because it was mainly a single-surface section. The unsuitability of this analysis for the Langley Aerodrome airfoil became apparent when the results showed high coefficients. This is because small angle assumptions made in the theory are not accurate for an airfoil that is highly cambered like the Langley Aerodrome airfoil. The maximum camber of the airfoil was $0.065c$, and the camber was strongly biased toward the leading edge with its maximum at $0.298c$ along the chord. This created a highly curved camber line near the leading edge. Also, the theory does not take into account viscous effects leading to flow separation. Another very important reason to find an alternative means to obtain the aerodynamic characteristics of the airfoil was that the main spar and trailing-edge spar could not be modeled in thin-airfoil theory analysis. These were placed on top of the wing skin surface of the Aerodrome, and they would definitely have had some influence on the airflow. Therefore, it was decided that wind-tunnel tests would be the most appropriate means for determination of the properties of the Langley airfoil.

Wind-Tunnel Model

Size and strength were important considerations when the wind-tunnel model was designed. First, the size was important because it had to fit into the test section; and it had to be large to achieve as high a Reynolds number as possible. The launch Reynolds number of the Langley Aerodrome wing was approximately 2.36×10^6.

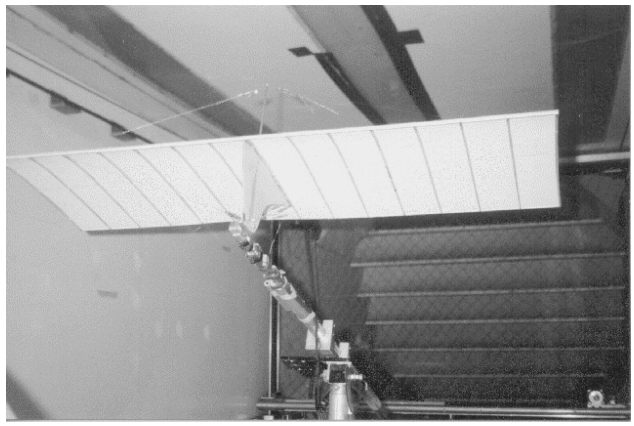

Fig. 7 Wind-tunnel model mounted in the subsonic wind tunnel.

This value is based on a launch speed of 9.75 m/s (32 ft/s) and a head wind of 5.36 m/s (12 mph) (Ref. 4). The scale of the ribs in the wind-tunnel model was approximately 1:12 that of the full-size Aerodrome. If the scale were reduced any further, it would have become much more difficult to recreate an accurate rib shape. Likewise, the model could not be made strong enough to withstand the aerodynamic loads, even at low airspeeds. The single-surface airfoil made it difficult to produce enough strength and stiffness in the model. It was necessary to add guy wires to the model (as, in fact, was needed for the full-sized wing). The final dimensions of the wind-tunnel model were 914 by 298 mm. Its aspect ratio was about 3.07, and the maximum Reynolds number achieved was approximately 3.09×10^5. The wind-tunnel model mounted on the balance in the wind tunnel is shown in Fig. 7. The side and top views of the rib from the Langley Memoir were used to design the model ribs. These were made with a rectangular cross section, even though the ribs on the Langley Aerodrome had six-sided cross sections at some points. It would have been too difficult to reproduce them exactly to scale. Seven layers of 0.397-mm (1/64-in.) plywood were laminated together to build each rib. The plywood plus the glue layers made the ribs approximately scale in height (about 3.4 mm).

A fiberglass rod was the best choice for the circular cross section front spar because it was very stiff and easy to glue. The main spar required extra strength and stiffness, and so steel music wire was used. Both of these spars were 3.175 mm (1/8 in.) in diameter. When the thickest part of the spars on the Aerodrome are scaled, a diameter of 3.167 mm results, and so it was a close match. A 1.588-mm (1/16-in-) diam fiberglass rod was sanded down into a D-shape for the trailing-edge spar. Fiberglass rods, 3.175 mm (1/8 in.) in diameter, were used for diagonal cross braces at the wing tips of the wind-tunnel model. They provided important structural support for the last two ribs, just as in the full-size Aerodrome.

A 3.175-mm- (1/8-in.-) thick plywood pylon and an aluminum bracket were used to mount the wing to a strain-gauge balance and to support the guy wires. The pylon can also be seen in Fig. 7 below the wing. The two upper and two lower guy wires used to support

the wing loads were made from 0.203-mm- (0.008-in.-) diam steel wire. The covering chosen for the model was Litespan, which is a light random-layup plastic paper made in England by Solarfilm. Tufts for flow-visualization tests were cut from Mylar® and were attached to the covering with clear adhesive tape. These tufts were approximately 3-mm wide and 38.1-mm long and were taped onto the top and bottom wing surfaces in a random scattered pattern.

Wind-Tunnel Testing Results

The University of Toronto Institute for Aerospace Studies subsonic wind tunnel was used for the tests. It is a closed-circuit design with a test section of 1.12 by 1.68 m. The operating range of wind speeds is from about 7 to 30 m/s. Force measurements were taken on the model by the use of a six-degree-of-freedom strain-gauge balance. The force measurement tests were conducted at angles of attack from −4 to 18 deg, at increments of 1 deg. Zero offset measurements were recorded for each angle and subtracted from the dynamic measurements. A Netdaq, made by Fluke Electronics, was used as the data-acquisition system for the wind-tunnel tests. It is capable of recording 20 analog channels and 10 digital channels. The sampling rate was set at continuous. On this setting, the Netdaq recorded 650 samples for the 6-s sample time (approximately 108.3 Hz). The samples were averaged over the sample time.

The results of the wind-tunnel force measurement tests, shown in Fig. 8, give the lift, drag, and pitching moment coefficients vs alpha. The lift coefficient data were approximately linear from −4 to 14 deg, and a linear curve fit produced a lift curve slope ($C_{L\alpha}$) equal to 0.0766/deg and an angle for zero lift of −1.34 deg. Those two values are important because they were used to determine the lift force for ANSYS models of the wing. The aerodynamic center of the airfoil was assumed to be at the quarter-chord position, and $C_{M_{ac}}$ is calculated about that point. The variation in $C_{M_{ac}}$ with angle of attack is likely due to stall and flow separation, which are described later.

The Lowry and Polhamus equation (see Ref. 6) was used to transform $C_{L\alpha}$ from the model's aspect ratio to the effective aspect ratio of the full-sized Aerodrome. The form of this equation, valid for arbitrary aspect ratios and wings with zero sweep and no Mach effects, is

$$C_{L_\alpha} = \frac{2\pi AR}{2 + \sqrt{4\pi^2 AR^2 / CL\alpha_\infty + 4}} \tag{1}$$

The influence on the lift curve slope of the gap between the wing halves of the Langley Aerodrome was accounted for by the use of an effective aspect ratio. A method for determination of this aspect ratio was found in Ref. 7. The data were produced for a wing with an aspect ratio of six, but it was still applied to the Langley wing because it was the only source available. The theory states that thickness of square and blunt wing ends becomes an obstruction to the flow through the gap at low ratios of y/c (where y is the gap dimension). The Aerodrome has a large gap, with a $y/c = 0.294$, and so the obstruction of flow between the wing halves is small, decreasing the effectiveness of each half. The y/c ratio is then used in the method to produce an effective aspect ratio of the wing. The result is a ratio of $(AR)_i/(AR)_o = 0.59$. Because $(AR)_o$ for the Langley wing was 3.842, the effective aspect ratio became 2.267. This result shows that the wing halves were not much more effective than two completely separate wings. Equation (1) was used to convert the $C_{L\alpha}$ of the wind-tunnel model to the infinite-aspect-ratio value $(C_{L\alpha})_\infty$ by the use of the model's aspect ratio. Then, it was converted a second time with the effective aspect ratio of the Aerodrome to obtain $(C_{L\alpha})_{\text{Aerodrome}} = 0.05885$/deg (3.372/rad).

$(C_{L\alpha})_{\text{Aerodrome}}$ was used to calculate the lift of the aerodrome. The initial angle of attack of the Aerodrome was 9 deg, taken from drawings in the Ref. 4. Based on that, sea-level air density, and the launch speeds already mentioned, the front wing alone could lift 359 kg (790 lbs.). This is very close to the total aircraft mass of 386 kg (850 lbs.). Without knowing the downwash effect on the rear wing, it is hard to estimate the total lift. However, the rear wing was mounted at the same angle of attack as the front, so that the Aerodrome may have had adequate lift for flight.

Pressure Measurement

Surface pressure measurements were taken on the wind-tunnel wing. The model was so thin that the conventional method of running pressure taps internally through the wing was impossible. Instead, the pressures were measured with an external probe pressed against holes right through the wing, so that the pressure on the upper surface could be measured from the lower surface, and vice versa. For example, the probe would be moved from one hole to another on the lower surface, sampling the pressures at the opening on the upper surface. The model modifications needed for this method involved making one central spanwise section from rigid material, so that the holes could be drilled through and the probe could be pressed against them without distortion of the shape of the airfoil. Most of the wing was only the thickness of the fabric covering, and so 0.397-mm- (1/64-in.-) thick plywood sheeting was chosen to stiffen the section with the pressure holes. The diameter of the holes was 0.794-mm (1/32-in.-), and the pressure probe was made so that it would affect the flow as little as possible. A brass tube 368-mm (14.5-in.-) long, with a 3.97-mm (5/32-in.-) outer diameter and about a 3.175-mm (1/8-in.-) inner diameter, was chosen. An analogue water manometer was used to measure the pressures from the probe. Pressure readings were taken at angles of attack of 6–9 deg and were converted into a $\Delta Cp(x)$ coefficient for each pressure tap. $\Delta Cp(x)$ was defined by

$$\Delta Cp(x) = \frac{\text{upper\_pressure}(x) - \text{lower\_pressure}(x)}{\frac{1}{2}\rho V^2} \tag{2}$$

The results of the measurements are presented in Fig. 9 in terms of $\Delta Cp(x)$, with $x = 0$ being the leading edge.

The upper surface had negative pressures all along its length. The lower surface had mainly positive pressures, except for the

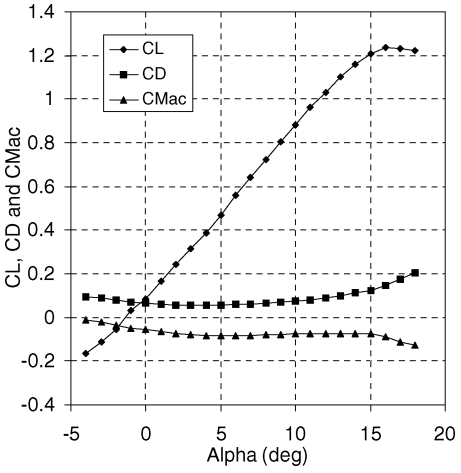

Fig. 8 Lift, drag, and pitching-moment coefficients vs alpha.

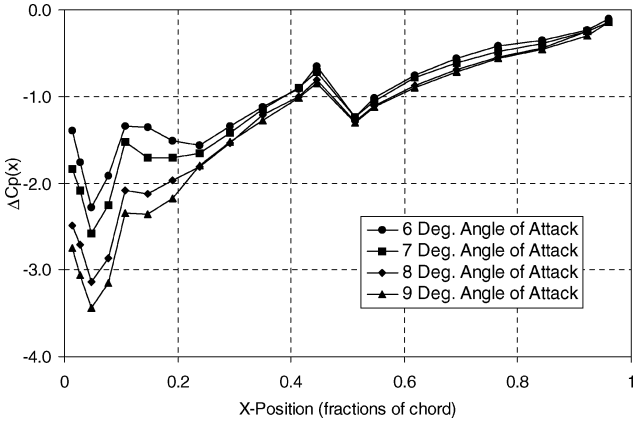

Fig. 9 Average $\Delta Cp(x)$ for 6–9 deg.

very last point. A jump in the pressure is visible just before 0.5*c*. This jump spanned the position of two pressure taps on either side of the main spar. Note that, when these pressure distributions are integrated over the mean camber line of the airfoil, they produce coefficients of different magnitude than the force measurement coefficients. The average difference for the four angles produces a 35% higher lift and a 17.6% lower pitching moment. There were two sources of error that could have contributed to these differences were obtained. The first was the presence of the probe affecting the airflow around the wing. The second was that an experimenter was required in the tunnel to move the external probe from one hole to another. Changes in dynamic pressure caused by this method were accounted for and the effect of the experimenter's position was investigated and minimized. This method was chosen because it was the quickest and simplest way for the pressures to be obtained.

The flow-visualization tufts showed that there was no angle of attack where both the upper and lower surface simultaneously had completely attached flow. The lower surface had separated flow behind the leading edge at every angle. The upper surface had separated flow at the main spar, just after 0.5*c*, at every angle. The least amount of separation occurred at angles of attack from 11 to 15 deg. The Aerodrome was designed to fly at an angle of attack of 9 deg.

ANSYS Wing Model Structural Analysis

Aeroelastic and structural analyses of the Langley Aerodrome wing were performed with ANSYS (ver. 5.0), a finite element code developed by Swanson Analysis Systems, Inc.[8] Detailed three-dimensional models of the wing were created, and two specific examples were studied, one with rigid ribs and one with nonrigid, or elastic, ribs. The rigid-rib case was created and analysed first, by the use of the wind-tunnel force and moment loads. The second case, with elastic ribs, was studied to obtain stress output in addition to displacement information. The wind-tunnel pressure distribution was used as the load on the elastic rib case. To simplify the aeroelastic analysis, macros were written to create the input, analyze the output, and carry out an iterative solution on the model. The ANSYS program also created an output of the forces and stresses on the wing. Figure 10 shows an example of an ANSYS wing model. The darkest lines in the plot are the guy wire elements, and the lighter lines represent the other element types that make up the model. The rib guy posts and the wires that ran over them from the leading edge to the trailing edge were unique to the elastic-rib model. The rigid-rib model did not need the conceptual structural support of these wires. The starboard wing was chosen as the numerical example. Its wing tip is at the lower left of Fig. 10, and the upper right of the wing is attached to the fuselage. The midrod, upper guy post, and lower guy post are part of the fuselage.

Several element types were used in the ANSYS wing model, including beam, tube, link (tension only for cables), and pin joint elements. Solid model elements were not used, because most members in the Aerodrome wing were long and fairly uniform. The elements were assigned real constants such as sectional moment of inertia, thickness, and diameter. Reference 4 was very thorough, and so only a few assumptions about geometry and materials had to be made.[9] In terms of material properties, the elastic modulus of the spruce and steel parts used was identified. A third material property was also defined for the rigid ribs. This assumed rigid material was given an elastic modulus with a magnitude five times that of steel, which makes the third material property essentially rigid.

The model consisted of 245 elements, along with nodes placed at strategic locations. That is, wherever members of the wing were joined, a node was needed. Attachments of ribs to spars, and guy wires to guy posts, were all locations of that kind. Wherever a force or constraint was applied, there had to be a node. The choice of nodes placed on the ribs involved two considerations. First, the curve of the ribs had to be re-created as closely as possible, and, second, the aspect ratio of sections of the tapered beam elements used was restricted in ANSYS. Control nodes were used for the pin joint elements to specify the direction of the pin axis. The locations of the nodes were measured or read from figures in Ref. 4.

Two types of constraints had to be placed on the model to simulate the way the wing was supported. The first type was a completely fixed support. All displacements and rotations of these nodes were constrained to be zero. Such nodes were those directly connected to the main frame of the Aerodrome fuselage. These include the nodes at the end of the front and main spars, the ones that attach the guy wires to the frame, and the ends of the upper and lower guy posts and midrod that attach to the frame. For other nodes along the aircraft-symmetry boundary, the forces in the y direction caused by each wing were equal and opposite, thus cancelling out. These nodes include the free ends of the upper and lower guy posts and the midrod, and they would only have displacements in the x–z plane of the constraint coordinate system.

Application of the Aerodynamic Loads

The loads applied to the wing model were functions of the angle of attack and were based on the wind-tunnel data. As the wing deformed, the angle of attack was calculated from the displacements of nodes at the leading and trailing edges of the wing. The aerodynamic effects of the rib deformation for the elastic-rib case were not accounted for in this analysis.

The Schrenk approximation,[10] was used to determine the spanwise lift distribution. It is a mathematical method that uses the planform shape and twist. It consists of two parts: a component without twist, and a twist component without net lift for twisted

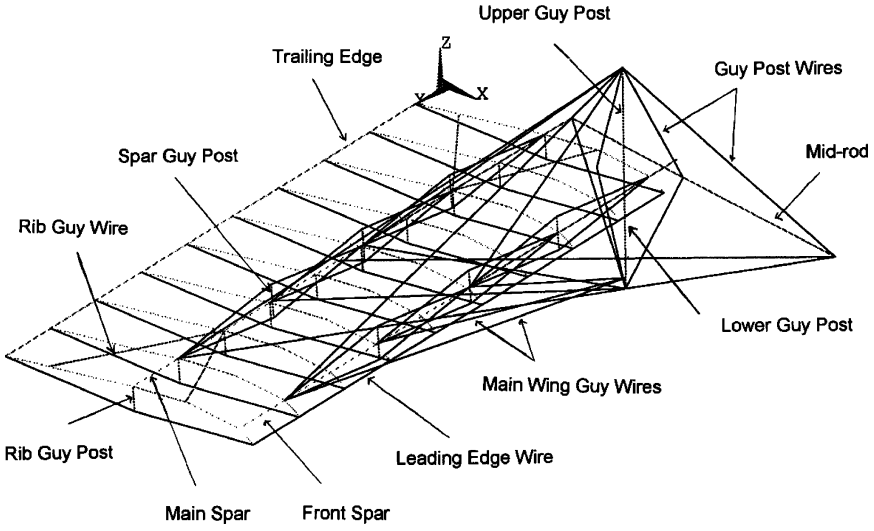

Fig. 10 Elastic-rib wing model.

wings. For the component without twist, the lift distribution is found when the chord distribution of the wing and a semi-ellipse of the same area are averaged. The twist component without lift is found by determination of the average angle of the twisted wing, followed by calculation of the effects of the difference in twist everywhere along the wing compared to the average. The equation presented by Schrenk is as follows:

$$\frac{dL}{dy} = \frac{1}{2}q\left(C_{L_\alpha}\right)_{\text{wing}}\alpha\left[c(y) + \frac{4}{\pi}\bar{c}\sqrt{1-\left(\frac{y}{b/2}\right)^2}\right] + \frac{1}{2}q\left(C_{L_\alpha}\right)_{\infty}\delta(y)c(y) \tag{3}$$

The first term on the right is the component without twist. The second term within the brackets is the equation of a quarter ellipse of the same area as the planform. The 1/2 outside the brackets averages the two. The second term is the twist component without lift. When this is integrated along the span of the wing the result is zero lift, which is the meaning of the without lift term.

The Schrenk approximation was applied in a special way for the Langley Aerodrome. The reason for this is the gap between the wing halves. The basic Schrenk method could be used to get a lift distribution of one isolated wing half with no influence of the other one-half, or it could be used to get a lift distribution of a full gapless wing. An assumption was made that the Aerodrome's lift distribution was some combination of the two because of the gap. Because the effective aspect ratio was used to determine $C_{L\alpha}$ for the Aerodrome wings, it was also used to obtain the lift distribution. The effective aspect ratio was 0.59 times the full-wing aspect ratio, or 1.18 times (18%) higher than the aspect ratio of one-half wing. It was assumed that the lift distribution had similar characteristics and that 82% of it must come from a Schrenk distribution for one-half wing, and 18% from a complete wing. The results of this are given by the following equation for the lift without twist portion:

$$\frac{dL}{dy} = q\bar{c}\left[\left(C_{L_\alpha}\right)\alpha\right]\frac{1}{2}\left\{0.18\left[1+\frac{4}{\pi}\sqrt{1-\left(\frac{y}{b/2}\right)^2}\right] + 0.82\left[1+\frac{4}{\pi}\sqrt{1-\left(1-\frac{y}{(b/2)/2}\right)^2}\right]\right\} \tag{4}$$

In the Eq. (4), $c(y)$ has been replaced with $\bar{c}$ for the rectangular wings. The equation was integrated over sections of the wing where the loads are applied to the ribs, resulting in the spanwise lift distribution. The local spanwise angle of attacks, determined during the structural analysis, were used in Eq. (4). It was assumed that the equation still applies, accounting for the twist using local angle of attacks.

The wind-tunnel pressure distribution loads were scaled to account for the spanwise location of the pressure measurements, the difference in aspect ratio between the wind-tunnel model and the Aerodrome wing and the spanwise distribution of the lift on the Aerodrome. The ΔCp values for the wing model were found by interpolation between the measured angles. Then those ΔCp values were divided by the Schrenk factor of 1.121 for the particular section of the wind-tunnel model where the measurements were taken, to convert the local pressure to a mean pressure for the wind-tunnel model. This mean pressure was then multiplied by the ratio of the lift curve slopes (found from wind-tunnel force measurements) to account for the aspect ratio difference between the mean lift of the wind-tunnel model and that of the Aerodrome. The equation for the preceding conversions results in a mean pressure distribution for the Aerodrome wing given by

$$\overline{(\Delta C_p)}_{\text{Aerodrome}} = (\Delta C_p)_{\text{WTM}}\frac{\left(C_{L_\alpha}\right)_{\text{Aerodrome}}}{\left(C_{L_\alpha}\right)_{\text{WTM}} \times 1.121} \tag{5}$$

Once this value is found, it can be distributed on a desired rib by another multiplication by a Schrenk factor for the Aerodrome lift distribution. The result is a pressure load for a particular rib given by

$$(\Delta C_p)_{\text{AerodromeRib}} = (\Delta C_p)_{\text{WTM}}\frac{\left(C_{L_\alpha}\right)_{\text{Aerodrome}}}{\left(C_{L_\alpha}\right)_{\text{WTM}} \times 1.121} \times \textit{Aerodrome\_rib\_Schrenk\_factor} \tag{6}$$

This method was repeated for each rib, and an example of the resulting distributed load is shown in Fig. 11. The force in Fig. 11 is presented per unit length because the ANSYS elements accept that form at their ends and distribute the load along the element.

An iterative aeroelastic deformation solution was used because the loads on the wing changed with deformation. Once a solution was found, a new set of loads had to be created and applied. A convergence criterion was chosen to determine when the iterations should stop, which is based on the change in wing twist at the ribs

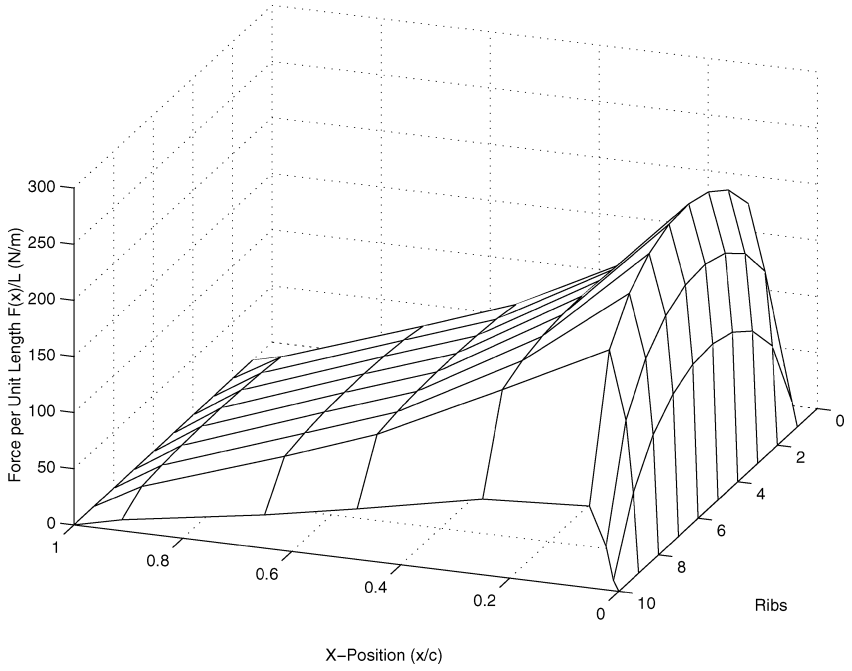

Fig. 11 Surface load.

between iterations, because the twisting drives the aeroelastic divergence. If the maximum iterative change in wing twist at all of the ribs was less than 0.05%, and the percentages decreased for subsequent iterations, then the solution was assumed to be converging. If the changes met these convergence criteria, it meant that the solution was reaching a steady state. Each iteration required an individual ANSYS solution that also had convergence criteria. To converge, the square root sum of the squares (SRSS) of the reaction loads had to be within 0.1% of the SRSS of the applied loads.

The ANSYS parametric design language provided a method for automation of the analysis by the use of combinations of ANSYS commands and calculations written in the FORTRAN programming language. It was used to calculate loads, apply loads, check convergence, and to postprocess.

Buckling and Stress Analysis

Nodal-force data and elemental stress information were produced in the postprocessing and used in the buckling and stress analysis. Buckling analysis was performed on the elements of the fully elastic ANSYS wing model. A buckling analysis of the rigid-rib model was not done because the loads were not distributed on the ribs and the resulting stresses were concentrated where the loads were applied. Euler buckling analysis was used on any element that met the required slenderness ratio criteria,[11] for which the critical buckling load is given by

$$P_{\text{cr}} = \pi^2 EI \big/ (L_e)^2 \tag{7}$$

Loads greater than P_{cr} imply failure. The effective length L_e of the member is determined by the end conditions.[12] Three types of end conditions were used: the semifixed–fixed with riveted or bolted ends, pin fixed, and fixed–fixed with perfectly rigid ends. The effective lengths for those end conditions are $0.82L$, $0.7L$, and $0.5L$, respectively. The equation used to determine the minimum slenderness ratio L/r required for Euler buckling is

$$L/r = \sqrt{\pi^2 E \big/ \sigma_{\text{cr}}} \tag{8}$$

In this equation, σ_{cr} was chosen to be the yield stress. Another buckling criterion was used for some steel elements that had intermediate slenderness ratios[11] with L/r greater than in Eq. (8) but lower than $L/r_{\min}$ given by

$$L/r_{\min} = \sqrt{2\pi^2 E \big/ \sigma_y} \tag{9}$$

The intermediate critical buckling load is then given by

$$P_{\text{cr}} = (\sigma_y / A)\left\{1 - \left[(L/r)^2 \big/ 2(L/r_{\min})^2\right]\right\} \tag{10}$$

When slenderness ratios were found to be too small for a particular element, buckling analysis was not performed. Short, thick members with low slenderness ratios are not as susceptible to buckling, and failure of those members would likely be dominated by yielding.[13]

The stress analysis of the wing model consisted of comparison of the yield stress of the material of every element to the stress found by ANSYS. The maximum stress found by ANSYS was used for the investigation of all beam elements, and this was defined as the sum of the axial stress plus the maximum bending stress. The principal stress was used for all tube elements, and the axial stress was used for all guy wire elements. Pin joint elements did not produce stress output.

ANSYS Wing Model Results

The iterative aeroelastic deformation method was applied to the rigid-rib case, and it was found that the wing, at the assumed launch speed, deformed into a stable shape. It did not show signs of aeroelastic divergence. Two variables were used to observe the deformation and to determine the convergence. These were the angles of the ribs (or the twist of the ribs as the loads were applied) and the change in these angles between iterations. Figure 12 shows these two variables, plotted against the iteration number, for a rigid-rib case. Rib 1 is closest the fuselage and rib 10 is at the wing tip.

Figure 12 shows that the rib twist angles level off as the number of iterations is increased. The absolute percent difference in rib angles between iterations approached zero as more iterations were completed. These were the indicators that the wing was not diverging

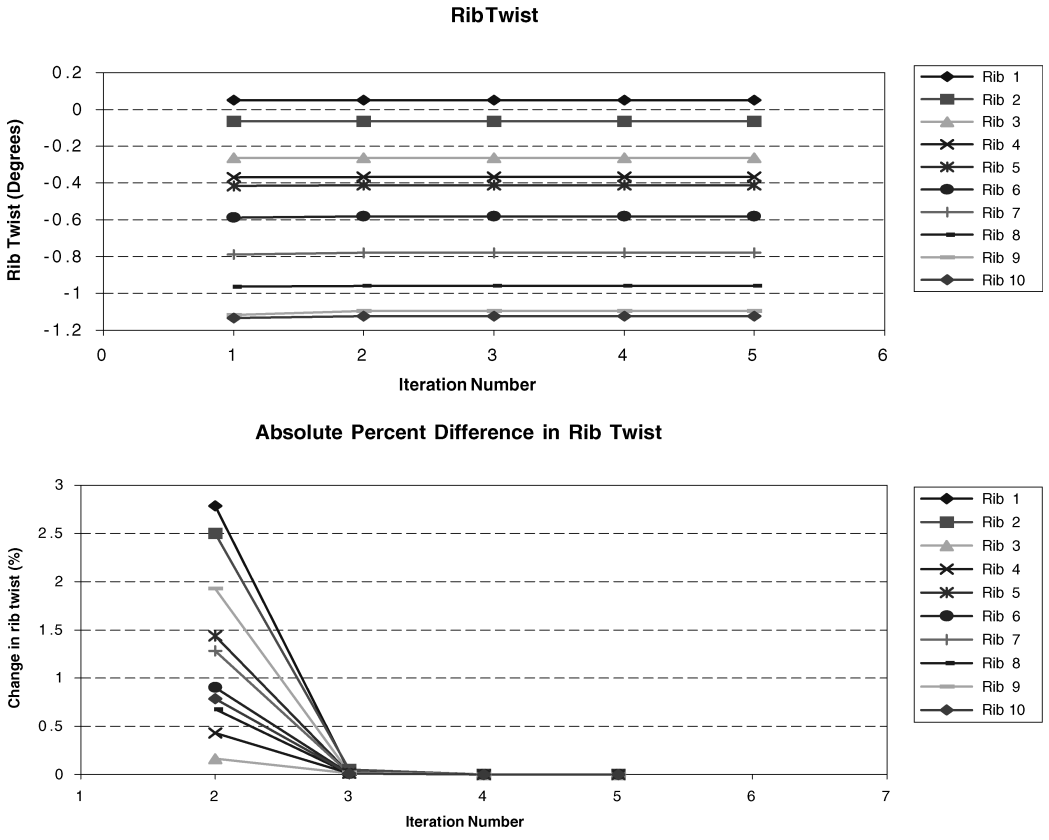

Fig. 12 Rigid-rib aeroelastic divergence results.

aeroelastically. Figure 13 shows the deformed wing shape. Note that it was created with the ANSYS program that exaggerates deformation to make it more visible. Therefore, the angles in Fig. 13 may not correspond to the actual twist angles in Fig. 12. Notice that the rib twist angles are mostly negative. Only the first rib has a small, positive twist. The entire wing is twisting in a clockwise direction as seen from above from the starboard wingtip. The maximum twist occurred at rib 10, which had a twist angle of −1.124 deg when the wing reached the converged deformed shape. The minimum absolute twist occurred at the second rib near the fuselage. Its twist angle was −0.0507 deg. The maximum absolute percent difference in the twist angle, between iterations 4 and 5, was $1.71e-5\%$, which showed that convergence had been attained.

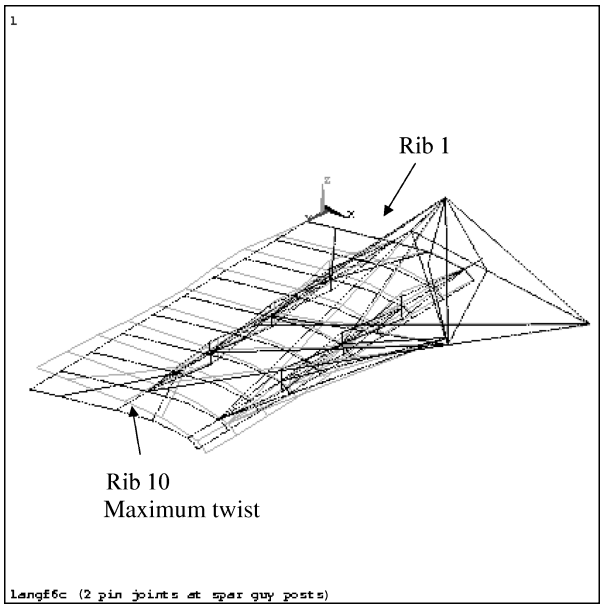

Fig. 13 Rigid-rib ANSYS wing-model deformation.

The results found in the elastic-rib case also did not show signs of aeroelastic divergence, and the wing converged into a stable deformed shape. Figure 14 shows the rib twist angles and percent differences for the iterations for the wind-tunnel pressure distribution. The maximum twist occurred at rib 7, with a twist angle of about −2.532 deg. The minimum twist occurred at the first rib, near the fuselage, with an angle of −0.355 deg. The maximum absolute percent difference in twist angle between iterations 6 and 7 was 0.00134% for the wind-tunnel pressure distribution. Figure 15 shows the deformation for the wind-tunnel pressure distribution. (Again, the deformations may be exaggerated.) The results were similar to those of the rigid-rib case where the trailing edge is twisted upward. The trailing edge of the Aerodrome's leading wing was also twisted up during the first launch attempt (Fig. 3).

In the elastic-rib case, the only member in the model that showed signs of buckling was the lower guy post. A force of 126% of the buckling load occurred for the wind-tunnel pressure distribution. It would have, thus, failed in some way. The stress output also identified elements with stresses higher than their yield stress. The elements that were overstressed were spar guy wires, with stresses of up to 140% of their yield stress. These guy wires were the ones supporting the main spar, nearest to the wing root. The wires supporting the front spar were also under high stresses, at up to 102% of their yield stress. The location of these wires was also nearest to the wing root. If the spar guy wires were to fail, the spar would likely be overloaded, which would lead to a complete wing failure.

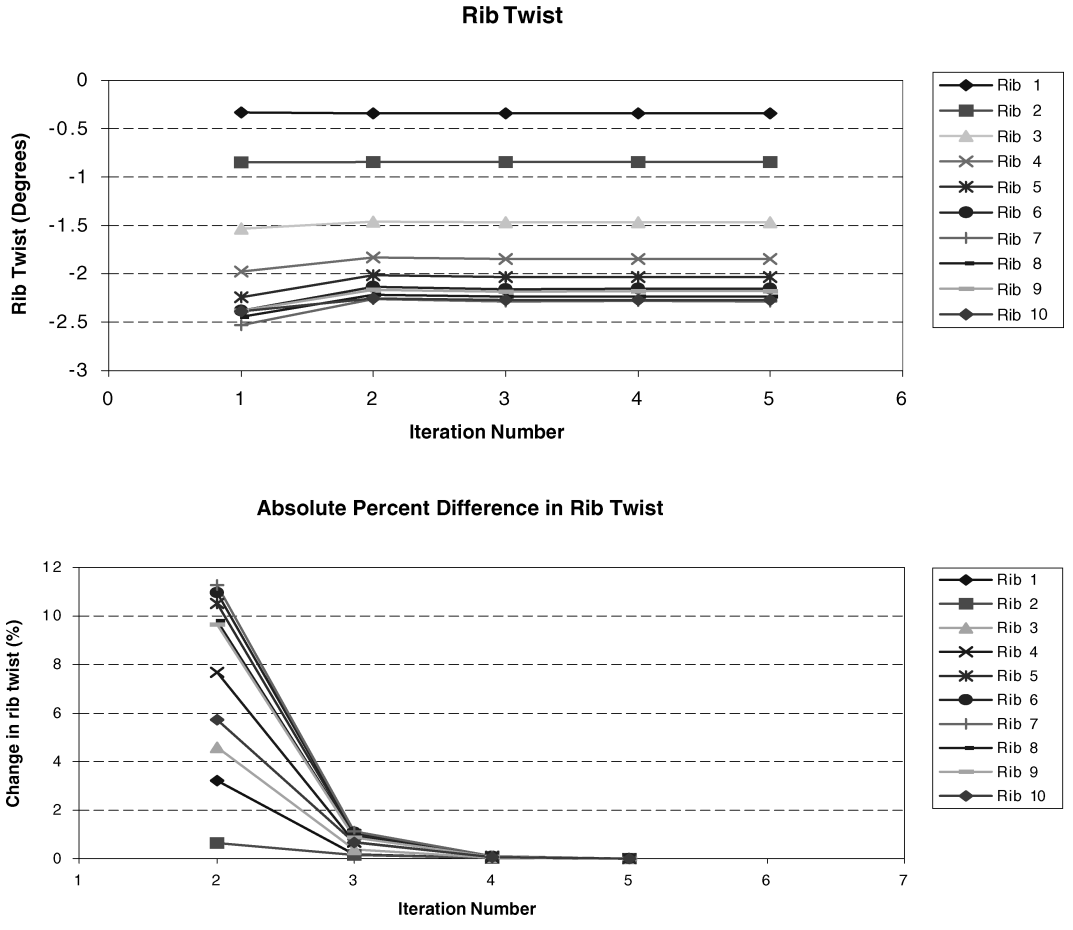

Fig. 14 Elastic-rib model with wind-tunnel pressure distribution divergence results.

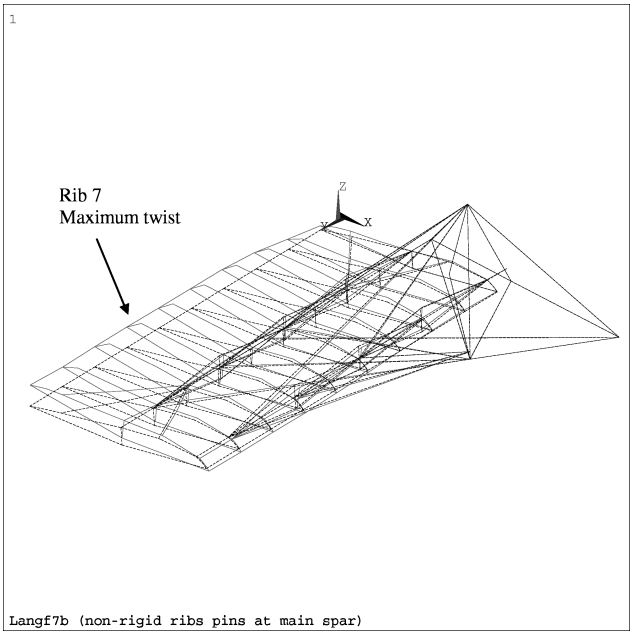

Fig. 15 Elastic-rib model deformation with wind-tunnel pressure distribution.

Conclusions

This paper described the aerodynamic and structural analysis of the Langley Aerodrome used to determine the cause of its failure on launch and to determine whether it was capable of flight. The following conclusions were made from this analysis:

1) The Langley Aerodrome wing did not fail because of aeroelastic divergence. The wing did, however, deform significantly. The main deformation was twist, with the leading edge bending down and the trailing edge bending up.

2) Part of the wing deformation was in the ribs themselves. The ribs bent upward at the trailing edge, which contributed to the twist of the wing. This, alone, could have changed the aircraft's trim state and resulted in instability.

3) The Langley Aerodrome wing was also not structurally capable of supporting the load imposed on it during the launch. The lower guy post was subjected to axial forces that were above its critical buckling load, and the guy wires supporting the main spar of the wing were subjected to stresses above their yield stress. Yielding of the guy wires would reduce their ability to support the main spar and cause structural failure.

In conclusion, the Great Aerodrome did not have the ability to fly, even with a perfect launch. This was a sad ending to an extraordinary quest by Samuel Langley. If future analysis were done on this aircraft, the aerodynamic model could be improved by the use of computational fluid dynamics. The aerodynamics of the deformed wing, including the ribs, could be determined and provide a more complete aeroelastic analysis.

Acknowledgments

The National Sciences and Engineering Research Council supported this research by providing a postgraduate scholarship. The authors would like to thank T. D. Crouch at the Smithsonian National Air and Space Museum for supplying technical information about the Aerodrome.

References

[1]Anderson, J. D., Jr., "The Infancy of Aerodynamics: To Lillienthal and Langley," *A History of Aerodynamics*, Cambridge Univ. Press, Cambridge, England, U.K., 1997, pp. 181–188.

[2]Wright, L., "Lorin Wright to Orville Wright, 4 June 1915," *The Papers of Orville and Wilbur Wright*, edited by M. W. McFarland, Vol. 2, 1906–1948, McGraw–Hill, New York, 1953, pp. 1087–1090.

[3]Bisplinghoff, R., Ashley, H., and Halfman, R., *Aeroelasticity*, Addison Wesley Longman, Reading, MA, 1955, p. 3.

[4]Langley, S. P., and Manly, C. M., *Langley Memoir on Mechanical Flight*, Smithsonian Inst., Washington, DC, 1911, pp. 161–206, 265, 271.

[5]Bertin, J. J., and Smith, M. L., *Aerodynamics for Engineers*, 2nd ed., Prentice–Hall, Englewood Cliffs, NJ, 1989, pp. 204–234.

[6]Lan, C.-T. E., and Roskam, J., *Airplane Aerodynamics and Performance*, Roskam Aviation and Engineering, Ottawa, KS, 1980, pp. 101, 102.

[7]Hoerner, S. F., *Fluid-Dynamic Drag*, S. F. Hoerner, Midland Park, N.J., 1965, pp. 7–15,7–16.

[8]*ANSYS User's Manual*, ver. 5.0, Vol. 1, Procedures, Swanson Analysis Systems, Inc., Houston, PA, 1992.

[9]Auriti, L., *Aeroelastic Analysis of the Langley Aerodrome*, M.S. Thesis, Inst. for Aerospace Studies, Univ. of Toronto, Toronto, ON, Canada, 1998, pp. 117, 118.

[10]Schrenk, O., *A Simple Approximation Method For Obtaining The Spanwise Lift Distribution*, NACA TM 948, April 1940.

[11]Beer, F. P., and Johnson, E. R., Jr., *Mechanics of Materials*, 2nd ed., McGraw–Hill, Toronto, ON, Canada, 1992, pp. 631–688.

[12]Raymer, D. P., *Aircraft Design: A Conceptual Approach*, AIAA, Washington, DC, 1992, pp. 374–377.

[13]Timoshenko, S., *Strength of Materials*, Part I Elementary Theory and Problems, 2nd ed., D. Van Nostrand, New York, 1940, pp. 250–255.